International Journal of Remote Sensing, 2013
Vol. 34, No. 20, 6969–6982, http://dx.doi.org/10.1080/01431161.2013.810825

Taylor & Francis
Taylor & Francis Group

A hybrid pansharpening approach and multiscale object-based image analysis for mapping diseased pine and oak trees

Brian Alan Johnson[a,b]*, Ryutaro Tateishi[a], and Nguyen Thanh Hoan[a,c]

[a]*Centre for Environmental Remote Sensing (CEReS), Chiba University, 1-33 Yayo-icho, Inage, Chiba 263-8522, Japan;* [b]*Institute for Global Environmental Strategies, 2108-11 Kamiyamaguchi, Hayama, Kanagawa 240-0115, Japan;* [c]*Institute of Geography, Vietnamese Academy of Science and Technology (VAST), 18-Hoang Quoc Viet, Hanoi, Vietnam*

(*Received 6 February 2013; accepted 8 May 2013*)

We developed a multiscale object-based classification method for detecting diseased trees (Japanese Oak Wilt and Japanese Pine Wilt) in high-resolution multispectral satellite imagery. The proposed method involved (1) a hybrid intensity–hue–saturation smoothing filter-based intensity modulation (IHS-SFIM) pansharpening approach to obtain more spatially and spectrally accurate image segments; (2) synthetically oversampling the training data of the 'Diseased tree' class using the Synthetic Minority Over-sampling Technique (SMOTE); and (3) using a multiscale object-based image classification approach. Using the proposed method, we were able to map diseased trees in the study area with a user's accuracy of 96.6% and a producer's accuracy of 92.5%. For comparison, the diseased trees were mapped at a user's accuracy of 84.0% and a producer's accuracy of 70.1% when IHS pansharpening was used alone and a single-scale classification approach was implemented without oversampling the 'Diseased tree' class.

1. Introduction

Insects cause significant damage to forested areas of Japan. The Japanese pine sawyer beetle (*Monochamus alternatus*) and the oak platypodid beetle (*Platypus quercivorus*) are responsible for the large majority of the damage (Food and Agriculture Organization of the United Nations Regional Office for Asia and the Pacific 2010). The pine sawyer beetle is the vector for the pinewood nematode *Bursaphelenchus xylophilus*, which causes Japanese Pine Wilt (JPW) disease (Kobayashi, Yamane, and Ikeda 1984), and the oak platypodid beetle is the vector for the fungus *Raffaelea quercivora*, which causes Japanese Oak Wilt (JOW) disease (Kubono and Ito 2002). JPW is spreading to higher-altitude and higher-latitude regions, and JOW is rapidly spreading in many regions of Japan, and thus preventing further expansion of these diseases is a high priority (Food and Agriculture Organization of the United Nations Regional Office for Asia and the Pacific 2010). In the summer, pine sawyer beetles and oak platypodid beetles emerge from trees killed the previous year, and then proceed to attack and nest over the winter in new trees, continuing this cycle (Ohta et al. 2012; Uto et al. 2011). Thus, rapid detection and removal or treatment of newly infected trees is necessary to prevent the beetles from emerging the following year and spreading

*Corresponding author. Email: bjohns53@fau.edu

the diseases. Foliage discolouration is a clear sign of JPW and JOW, so the detection of a diseased tree is typically associated with the detection of a discoloured tree. However, in areas of Japan with cool summer weather, *B. xylophilus* can become latent, causing a delay or absence of symptoms (e.g. discolouration) in pine trees infected with JPW (Futai 2003). Nonetheless, the pine trees in these cool summer regions that exhibit discolouration between July and October have been found to be the most important targets for preventing JPW from spreading (Ohta et al. 2012). In this study, we focus on mapping trees with discoloured foliage, using multispectral satellite imagery acquired in late August.

Previous remote sensing studies have found that high-spatial resolution imagery is needed for detecting JPW and JOW at the individual tree level (Komura et al. 2003; Lee and Cho 2006). In true colour images the discoloured trees appear more red-to-brown in colour than surrounding trees. Past research has used high-spatial resolution hyperspectral images from airborne sensors to detect JOW (Dellerba 2010), but these images are generally expensive to acquire and the size of the data is quite large due to the high number of spectral bands. Since it is relatively easy to visually identify discoloured trees in true colour and colour-infrared images, hyperspectral imagery may not be needed for image classification. High-resolution multispectral images acquired from spaceborne sensors such as QuickBird, GeoEye-1, or WorldView-2 are less expensive and easier to acquire than airborne hyperspectral images, so developing a method for detecting JPW and JOW in this imagery would be more useful for practical applications. However, no past studies of which we are aware have quantitatively assessed the accuracy at which JPW or JOW could be mapped in multispectral imagery. Additionally, no past studies have used an object-based image analysis (OBIA) approach, which typically performs better than a pixel-based approach for classifying high-resolution images (Blaschke, Burnett, and Pekkarinen 2004; Yu et al. 2006; Myint et al. 2011).

In this study, we developed a new method for detecting diseased pine and oak trees in high-resolution multispectral satellite imagery. First, the imagery was pansharpened using an intensity–hue–saturation (IHS) pansharpening approach because it has been found to lead to accurate image segmentations in previous research (Johnson, Tateishi, and Hoan 2012). Next, we adopted a multiscale OBIA approach (Johnson 2013) to incorporate preliminary support vector machine (SVM) classification results (class assignments and posterior probabilities) from many segmentation levels into a final land cover classification. The land cover types of interest, diseased pine and oak trees, were sparse compared with the other land cover in the study area, so collecting training data for this class was more difficult and time consuming. As a result, we had a highly imbalanced training data set, with training data for the target class comprising only 1.7% of the total training set. Highly imbalanced training data sets have been shown to result in lower classification accuracy for the minority class (Solberg and Solberg 1996), so prior to SVM classification we used the Synthetic Minority Over-sampling Technique (SMOTE, Chawla et al. 2002) to artificially oversample the minority class. Finally, since IHS pansharpening results in spectral distortion, we tested the effect of replacing the IHS spectral information of image segments with (i) the original multispectral information and (ii) the spectral information from another pansharpening algorithm, Smoothing Filter-based Intensity Modulation (SFIM; Liu 2000), which preserves spectral information better than IHS pansharpening. Our main findings were that (1) the use of a multiscale OBIA approach outperformed the single-scale OBIA approach; (2) performing SMOTE prior to image classification led to higher classification accuracy; and (3) replacing IHS spectral information with the original multispectral or SFIM spectral information also resulted in higher classification accuracy.

1.1. Pansharpening methods

High-spatial resolution spaceborne sensors such as QuickBird, GeoEye-1, and WorldView-2 acquire images with a few multispectral (MS) bands and a finer resolution panchromatic (PAN) band. For these types of images, 'pansharpening' image fusion methods are often performed to improve the spatial resolution of the MS bands using the PAN band (Schowengerdt 2006). Due to its speed and ease of implementation, IHS is one of the most commonly used pansharpening methods (Tu et al. 2001). IHS is very efficient at enhancing the spatial information of MS bands – it preserves all of the PAN band's spatial details (Tu et al. 2001). The main problem with IHS pansharpening is that it distorts the spectral information of the MS bands (Tu et al. 2001). An IHS pansharpening algorithm for four-band images is given by Tu et al. (2004) as

$$\begin{bmatrix} B'_{ihs} \\ G'_{ihs} \\ R'_{ihs} \\ NIR'_{ihs} \end{bmatrix} = \begin{bmatrix} B + \delta_i \\ G + \delta_i \\ R + \delta_i \\ NIR + \delta_i \end{bmatrix}, \tag{1}$$

where $\delta_i = PAN - I$ and $I = \alpha_1 \times B + \alpha_2 \times G + \alpha_3 \times R + \alpha_4 \times NIR$, B'_{ihs} is the pansharpened value for the blue band, B is the digital number (DN) value of the pixel in the original blue band (radiance or reflectance values can be used alternatively), and PAN is the DN of the pixel in the PAN image. G, R, and NIR refer to the DN values of the green, red, and near infrared bands, respectively. To minimize spectral distortion caused by the mismatch between the spectral response of the PAN and MS bands, band weights (α_1 to α_4) used for calculating intensity (I) can be adjusted based on the spectral response curve of the sensor (i.e. low weight given to MS bands with little overlap with the PAN band, and vice versa). However, even after adjusting I, significant spectral distortion may exist (Johnson, Tateishi, and Hoan 2012).

On the other hand, SFIM is a pansharpening algorithm that is very good at minimizing the distortion of MS information (Tu et al. 2012). However, it does not enhance the spatial information of the MS bands to the same degree as IHS. Unlike IHS, SFIM can be applied to a four-band image without requiring α_1 to α_4. Instead, a smoothed version of the PAN band, typically obtained using a 7×7 mean filter (Tu et al. 2012), is used. SFIM can be calculated as

$$\begin{bmatrix} B'_{sfim} \\ G'_{sfim} \\ R'_{sfim} \\ NIR'_{sfim} \end{bmatrix} = \frac{PAN}{PAN_{smooth}} \times \begin{bmatrix} B \\ G \\ R \\ NIR \end{bmatrix}, \tag{2}$$

where B'_{sfim} is the pansharpened value for the blue band and PAN_{smooth} is the DN value of the pixel in the PAN band after the 7×7 mean filter has been applied. Thus, any change in the spectral information of the MS bands is caused solely by PAN/PAN_{smooth}. This SFIM equation is very similar to the 'smart mode' of the Hyperspherical Color Sharpening (HCS) algorithm (Padwick et al. 2010) developed for WorldView-2 imagery.

In a previous study, Johnson, Tateishi, and Hoan (2012) found that IHS pansharpened images produced segmentations that were more spatially accurate, while SFIM better preserved the spectral information of image segments. Based on these findings, a hybrid IHS-SFIM approach was recommended for OBIA. However, in the previous study, no image classification was done to confirm that a hybrid pansharpening approach could

actually achieve a more accurate classification. So, one important contribution of this study was that we tested hybrid pansharpening approaches for OBIA to assess their impact on classification accuracy.

1.2. Multiscale OBIA

OBIA, which involves segmenting an image into relatively homogeneous regions (i.e. 'image segments' or 'image objects') prior to image classification, has been shown to increase classification accuracy by incorporating the spectral (e.g. mean) and non-spectral (e.g. texture, size, shape) information of image segments for classification (Blaschke, Burnett, and Pekkarinen 2004; Yu et al. 2006; Myint et al. 2011). The average size and/or homogeneity of image segments is typically determined by user-defined segmentation parameters, but since objects of interest in an image often differ in size and/or texture, use of multiscale information can result in higher classification accuracy (Bruzzone and Carlin 2006; Duro, Franklin, and Dubé 2012; Johnson 2013). Multiscale object-based classification approaches can be generally placed into two categories: (1) rule-based classification approaches based on expert knowledge (e.g. Zhou and Troy 2009), and (2) approaches that use automated classification algorithms like SVM (Bruzzone and Carlin 2006; Johnson 2013) or random forests (Duro, Franklin, and Dubé 2012). We focus on the second category, since the more automated methods are less subjective and more straightforward to apply to other study areas.

One popular multiscale classification approach involves (1) assigning the spectral and spatial information of image segments from coarser segmentation levels to the pixels (Bruzzone and Carlin 2006) or finer-scale image segments (Duro, Franklin, and Dubé 2012) that they contain, and (2) using this multiscale information to classify the finest-scale segments. Another multiscale approach uses posterior probability estimates from the preliminary classifications of multiple image segmentation levels to perform a final classification (Johnson 2013). In this approach, the different segmentation levels are hierarchically linked (i.e. the finest-scale segments are linked to the segments they are contained by in the coarser segmentation levels) to allow for multiscale analysis of the preliminary classification results (class assignments and posterior probabilities), and the final class assignment is performed for the finest-scale segments by identifying the class with the highest posterior probability.

2. Study area and data

Our study area (approximately 3.0 km × 2.5 km) was located near Yonezawa City in Yamagata Prefecture, Japan, and consisted mainly of deciduous broadleaf forest and evergreen needleleaf forest, with smaller areas of clear-cut forest and residential and agricultural land. This location was chosen because it contained many diseased oak and pine trees, and also because the area contained many other types of land use and land cover typically located near forests in Japan (e.g. residential areas, agricultural areas with a mixture of barren and vegetated fields). New occurrences of JOW and JPW in the region can generally be observed between June and October (Kobayashi, Yamane, and Ikeda 1984; Uto et al. 2011; Ohta et al. 2012), so we acquired a high-resolution QuickBird image of the study area from 27 August 2012 to detect the diseased trees. The QuickBird image contained four 2.4 m resolution MS bands (B, 0.450–0.520 μm; G, 0.520–0.600 μm; R, 0.630–0.690 μm; NIR, 0.760–0.900 μm) and a 0.6 m PAN band (0.445–0.900 μm).

3. Methods

3.1. Pansharpening

The QuickBird image was orthorectified using a 10 m resolution digital elevation model. After orthorectification, the image was pansharpened using the IHS algorithm in Equation (1). We chose to apply this pansharpening algorithm to the image prior to image segmentation because its ability to enhance the MS spatial information to a high degree was found to be beneficial for segmentation in previous research (Johnson, Tateishi, and Hoan 2012). To minimize the spectral distortion caused by the mismatch between the spectral response of the PAN and MS bands, band weights (α_1 to α_4) for calculating I in Equations (1)–(3) were set to 0.25, 0.75, 1, and 1, respectively, based on the simple spectral adjustment IHS approach recommended for QuickBird imagery in Tu et al. (2005).

3.2. Image segmentation

After pansharpening, the image was segmented using the 'Multiresolution Segmentation' algorithm in eCognition Developer 8.7 (Trimble 2012). This algorithm contains three user-defined segmentation parameters: a 'Scale parameter' (range 0–∞) that controls the maximum heterogeneity of image segments, a 'Shape' parameter (range 0–1) that controls the weights of spectral and spatial information in the segmentation process, and a 'Compactness' parameter (range 0–1) that controls the compactness of image segments (Trimble 2012). We used the IHS pansharpened G, R, and NIR bands for segmentation, but did not include the B band since it was highly correlated with the G band. Image segmentation was performed at four scale levels by adjusting the Scale parameter from 15 to 30 in steps of 5. For the remainder of this article, the four segmentation levels are referred to as scale 15 segmentation, scale 20 segmentation, scale 25 segmentation, and scale 30 segmentation for the sake of simplicity. The segments in the finer segmentation levels were completely contained by segments in the coarser segmentation levels (i.e. segments from different segmentation scales did not intersect one another). Use of multiple segmentation scales was necessary because not all diseased trees were segmented optimally at any single scale. Scale parameters lower than 15 were not used because they resulted in excessive oversegmentation of diseased trees (i.e. segments were much smaller than the diseased trees), and Scale parameters higher than 30 were not used because they resulted in undersegmentation of the diseased trees (i.e. segments were larger than the diseased trees, so they also contained other types of land cover). Since the trees were not uniform in shape, the Shape parameter was set to a very low level (0.1) for all segmentations to allow for spectral information to have a very high weight, and the Compactness parameter was set to 0.5 so that neither compact nor non-compact segments were favoured. These shape and compactness settings are typical for multispectral images because, in most cases, spectral information is most useful for creating meaningful segments (Trimble 2012).

The pixels located within an image segment were used to calculate the spectral information of the segment (e.g. mean value of each band, standard deviation of each band). For each image segment, we calculated mean spectral values for the G, R, and NIR bands as well as two commonly used texture metrics; standard deviation and grey-level co-occurrence matrix (GLCM) mean (all directions) (Haralick, Shanmugam, and Dinstein 1973). The B band was again excluded from analysis because of its high correlation with the green band, and the PAN band was used for both texture calculations because it contained the most detailed spatial information.

3.3. Training and validation data

After segmentation, training data were collected for two land cover classes 'Diseased tree' and 'Other', based on visual inspection of the imagery. The training data consisted of 4339 image segments. Many training segments were taken from each of the four segmentation levels, and the same training segments were used for classifying all four segmentation levels. We found that collecting training data for the target class 'Diseased tree' was difficult and time consuming because (1) this class comprised only a small part of the image and (2) we needed to identify segments with boundaries that accurately matched the boundaries of diseased trees in the image (since the training segment should have a good one-to-one relationship with a diseased tree). On the other hand, collecting training data for the 'Other' class was fast and easy since we could simply identify a few locations with no diseased trees and then select a large number of training samples at each of these locations. For the 'Other' class, we determined that it was not necessary for the training segment boundaries to accurately match the boundaries of land cover objects because the class was only intended to provide examples of segments that were not diseased trees. For the 'Diseased tree' class, we selected 74 training segments from the four segmentation levels. Of these 74 training segments, 37 were from scale 15 segmentation, 17 were from scale 20 segmentation, 10 were from scale 25 segmentation, and 10 were from scale 30 segmentation. For the 'Other' class, we selected a much larger number of training segments (4265) to ensure that the main land cover types in the image were included in the training set. Of these 4265 training segments, approximately 25% were taken from each segmentation level. Training segments taken from the four segmentation levels were all merged into a single training set that was used for classification purposes.

To assess image classification accuracy, 500 validation points were generated using a stratified random sampling approach (stratified by classified land cover). This sampling approach was chosen to ensure that the 'Diseased tree' class was adequately sampled. The validation set consisted of 187 points belonging to the 'Diseased tree' class and 313 points belonging to the 'Other' class (based on visual interpretation of the imagery). The validation points were used for calculating overall classification accuracy as well as producer's (e.g. errors of omission) and user's accuracies (e.g. errors of commission) for the 'Diseased tree' class. An image segment was determined to be correctly classified if it was assigned to the same class as the validation point found within it.

3.4. Replacing IHS spectral information

We tested the effect of replacing the IHS spectral values of image segments with (1) the original MS spectral information and (2) the SFIM spectral information. The anticipated result was that replacing the IHS spectral information would lead to higher classification accuracy due to less spectral distortion. The spectral replacement process for (1) was done by overlaying image segments onto the unsharpened MS image (i.e. the MS image with pixels upsampled to 0.6 m using nearest neighbour resampling) and then calculating the new spectral information of image segments from the pixels located within the segments. Likewise, the spectral replacement for (2) was done by overlaying image segments onto the SFIM pansharpened image and calculating segment values from the SFIM pixels. Figure 1 shows the process used to replace the IHS spectral information of segments with SFIM spectral information.

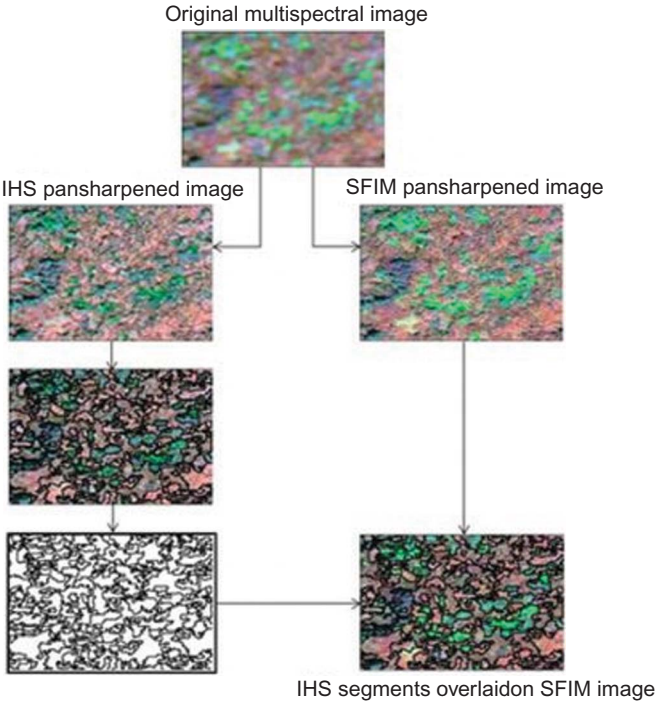

Figure 1. Spectral replacement process. In this example, the IHS image is segmented and then the spectral information of the image segments is extracted from the SFIM image (rather than the IHS image). Diseased trees appear white-to-grey in colour.

3.5. Minimizing effects of imbalanced training data set

Since our training data set was highly imbalanced, some classification algorithms will simply assign all (or almost all) segments to the majority class to achieve a high overall classification accuracy (Solberg and Solberg 1996). For example, since 98.3% of the training segments belonged to the 'Other' class, a very high overall accuracy is achieved simply by assigning all segments to that class. This is problematic since the minority class is the one that is of interest. If too many segments are assigned to the 'Other' class, a large number of diseased trees will not be mapped (i.e. low producer's accuracy). To increase the producer's accuracy of the minority class, we over-sampled it using SMOTE. SMOTE takes a training sample in the minority class and introduces new synthetic examples in the feature space between that training sample and one or more of its nearest neighbours in feature space, and then repeats this process for the entire training data set (Chawla et al. 2002). SMOTE has two free parameters; the number of nearest neighbours and the percentage of new training samples to create. For example, if the number of neighbours is set to 5 and the number of new training samples is set to 100%, the five nearest neighbours to a given training sample will be identified, and one new training example will be created between in the feature space between the original sample and one of the five nearest neighbours (randomly selected). Using SMOTE in this way would double the size of the training set for the minority class. For this study, we used the nearest 5 neighbours based on Chawla et al. (2002), and set the number of new training samples to 100% because, as shown later in Sections 4.1 and 4.2, the producer's accuracies for the 'Diseased tree' class were increased

to about the same level as the user's accuracies after doubling the size of the training data set.

3.6. Preliminary single-scale image classifications

Preliminary classifications of the four segmentation levels were done using SVM, a machine-learning algorithm that identifies the optimal decision boundary between classes to minimize classification errors (Burges 1998). SVM has been used for classification in many recent remote sensing studies (Mountrakis, Im, and Ogole 2011), and it tends to be more accurate for imbalanced data sets than other algorithms because only the samples close to the decision boundary (i.e. the Support Vectors) are used for classification (Tang et al. 2009). Prior to classification, a kernel is applied to the input feature space to increase the separability between land cover classes. Details about the commonly used SVM kernels in remote sensing are given by Kavzoglu and Colkensen (2009). In this study, we used SVM with a radial basis function (RBF) kernel for classification because it has achieved higher classification accuracy than other kernels in previous remote sensing studies (Foody and Mathur 2004; Kavzoglu and Colkenson 2009). The free parameters for SVM – the cost parameter (c) and the kernel spread function (γ) – were optimized for each segmentation by 10-fold cross-validation of the training data. We tested c values of 1.25^{-2}, 1.25^{-1}, . . ., 1.25^{31} and γ values of 1.25^{-30}, 1.25^{-29}, . . ., 1.25^{25}. To allow for posterior probability estimation, logistic regression models were fitted to the output of the SVM classifications, and posterior probabilities were calculated using Hastie and Tibshirani's (1998) pairwise coupling method. The final result of the preliminary classification process was that, in each of the four segmentation levels, all image segments received a class assignment and a probability estimate for that class (e.g. a segment classified as 'Diseased tree' with a probability estimate of 0.85 has an 85% chance that it is actually a diseased tree). All classification tasks were done using Weka 3.7.7, an open source data mining software package (Hall et al. 2009). In this study, we tested the traditional SVM classification method (i.e. without preprocessing the training data using SMOTE) and SVM with SMOTE preprocessing (SMOTE-SVM).

3.7. Multiscale classification

To allow for multiscale analysis of the preliminary classification results, a series of spatial joins was performed in ArcGIS 10 to provide the base classification units (i.e. the scale 15 segments) with the class assignments and posterior probabilities of the segments in which they were contained in each of the three coarser segmentations. Next, the final classification was done for each of the base units by identifying the segmentation level at which the highest posterior probability was achieved, and then assigning the base unit to the class to which the highest probability corresponded. A simple example of this classification process is shown in Table 1. Classification was done as the preliminary results from each of the coarser segmentation levels were added to the base units (i.e. when classes and posterior probabilities from scale 20 segmentation were passed on to the base units, and then again when scale 25 classes and probabilities were added, etc.) to determine whether accuracy decreased due to the undersegmentation of diseased trees in the coarsest segmentation levels. For the multiscale classifications, we used only the SMOTE-SVM classifications since, as discussed in Section 4.1, they were generally more accurate than the classifications without SMOTE.

Table 1. Example of the multiscale classification process.

Segment ID	True land cover	Classified land cover (scale 1)	Posterior probability (scale 1)	Classified land cover (scale 2)	Posterior probability (scale 2)	Highest posterior probability	Final classification (scale 1)
1	Diseased tree	Diseased tree	0.497	**Diseased tree**	**0.831**	0.831	**Diseased tree**
2	Other	**Other**	**0.892**	Diseased tree	0.493	0.993	**Other**
3	Diseased tree	Other	0.948	**Diseased tree**	**0.991**	0.991	**Diseased tree**

Notes: 'Scale 1' indicates the finest-scale segmentation level and 'Scale 2' indicates a coarser-scale segmentation level (i.e. segments that contain the Scale 1 segments). The column highlighted in grey shows the actual (ground truth) land cover. Bold text indicates the class with the highest posterior probability for each segment.

4. Results and discussion

4.1. Single-scale classifications

For the single-scale classifications, our main findings were that (1) the use of SMOTE typically increased all types of classification accuracy and (2) replacing the IHS spectral information of image segments with the MS or SFIM spectral information also resulted in higher classification accuracies. From Table 2, we can see that the segmentation with the highest overall accuracy and the best balance between producer's and user's accuracies for the 'Diseased tree' class was the scale 15 SMOTE-SVM classification with MS spectral information. Comparison of the classification accuracies at each scale using the different spectral information shows that MS and SFIM spectral information typically resulted in much higher overall and producer's accuracies. User's accuracy increased slightly when MS information was used, and a small decrease in user's accuracy occurred when SFIM information was used (though this decrease was minor compared with the increase in producer's accuracy). In Table 2 it is also clear that, while SMOTE typically increased producer's accuracies significantly in the finest-scale segmentation levels, producer's accuracies remained low in the coarser segmentation levels. This was likely due to the undersegmentation of many diseased trees in these coarse segmentation levels rather than imbalanced training data, since undersegmented diseased trees were difficult to detect when located within segments that also contained other types of land cover, resulting in many omission errors.

The results of the preliminary classifications suggest that SMOTE-SVM may be useful for binary classification of remote sensing images using object-based image analysis, especially in cases where it is relatively fast and easy to acquire training segments for the 'Other' land cover class. Other remote sensing studies have recommended using one-class classification algorithms for binary classification when training data for the 'Other' class is difficult and/or time consuming to acquire (Li, Guo, and Elkan 2011), as these one-class algorithms only require training samples for the class of interest. However, one-class classification methods that do not include any training data for the 'Other' class may result in low classification accuracy (Scott and Blanchard 2009) and/or have free parameters that are difficult to optimize (Manevitz and Yousef 2001; Muñoz-Marí et al. 2010). We do not compare SMOTE-SVM with one-class classifiers in this study, but suggest that researchers take into account the difficulty (or ease) of acquiring training data for the 'Other' class when choosing the optimal algorithm for a binary classification.

Table 2. Classified single-scale segmentations.

Spectral information	Segmentation scale	No SMOTE			SMOTE		
		OA (%)	UA (%)	PA (%)	OA (%)	UA (%)	PA (%)
Intensity–hue–saturation (IHS)	15	81.0	83.3	61.5	83.8	84.0	70.1
	20	78.4	89.1	48.1	81.6	91.3	56.1
	25	74.8	93.0	35.3	76.0	93.5	38.5
	30	71.4	97.9	24.1	72.0	98.0	25.7
None (original multi-spectral image)	15	86.6	86.6	75.9	90.0	88.7	84.0
	20	83.2	91.2	61.0	87.6	94.3	71.1
	25	79.4	92	49.2	83.4	95.6	58.3
	30	75.8	95.8	36.9	78.6	98.8	43.3
Smoothing filter-based intensity modulation (SFIM)	15	86.2	73.6	98.4	83.6	72.5	90.4
	20	85.2	86.0	72.2	85.0	85.9	71.7
	25	81.6	92.8	55.1	82.6	92.4	58.3
	30	76.2	96.0	38.0	77.8	96.3	42.2

Notes: SMOTE, Synthetic Minority Over-sampling Technique; OA, overall accuracy; UA, user's accuracy of the 'Diseased tree' class; PA, producer's accuracy of the 'Diseased tree' class.
Row highlighted in grey shows the most accurate classification.

4.2. Multiscale classifications

For the multiscale classifications, our main findings were that (1) using the multiscale approach increased all measures of accuracy and (2) replacing IHS spectral information with MS or SFIM information also led to higher classification accuracy. In this section, we describe these results in more detail and discuss how they compare with the results of past remote sensing studies.

As shown in Table 3, the multiscale classification with the highest overall accuracy and best balance between user's and producer's accuracies for the 'Diseased tree' class was the one with SFIM spectral information and the preliminary classification results from all four segmentation scales. The map of the diseased trees produced by this classification is shown for the entire study area in Figure 2 and for a subset of the area in Figure 3. The maps show, in general, a good match between the discoloured trees in the imagery (the reddish-brown areas in the forest) and the classification result.

Comparing the most accurate classifications for each pansharpening method, we found that replacing the IHS spectral information with MS and SFIM spectral information led to an increase in overall accuracy of 3.6% and 6.0%, respectively, and an increase in producer's accuracy of 10.2% and 18.7%, respectively, for the 'Diseased tree' class. The user's accuracy decreased slightly when IHS spectral information was replaced, but the decrease (0.6% for MS and 2.7% for SFIM) was minimal compared with the increase in producer's accuracy. These results confirm that replacing IHS spectral information can lead to higher classification accuracy. Thus, we recommend the use of a hybrid pansharpening approach for object-based classification of images with MS and PAN bands. Pansharpening methods that enhance spatial details are recommended for segmentation since they tend to produce more spatially accurate image segments (Johnson, Tateishi, and Hoan 2012), and pansharpening methods that minimize spectral distortion (or use of the original MS spectral information) are recommended for extracting the spectral information of segments.

Our finding that classification accuracy increased when a multiscale approach was used is consistent with past OBIA studies (Bruzzone and Carlin 2006; Duro, Franklin, and Dubé

Table 3. Multiscale classifications (e.g. 15–25 indicates that scale 15, 20, and 25 preliminary classifications were used for the multiscale classification).

Spectral information	Segmentation scale(s)	OA (%)	UA (%)	PA (%)
	15	83.8	84.0	70.1
IHS	15–20	88.0	93.2	73.3
	15–25	89.2	96.5	73.8
	15–30	90.0	99.3	73.8
	15	90.0	88.7	84.0
MS	15–20	93.0	95.8	85.0
	15–25	93.2	97.5	84.0
	15–30	93.6	98.7	84.0
	15	83.6	72.5	90.4
SFIM	15–20	92.8	88.7	92.5
	15–25	95.2	94.5	92.5
	15 – 30	96.0	96.6	92.5

Notes: OA, overall accuracy; UA, user's accuracy of the 'Diseased tree' class; PA, producer's accuracy of the 'Diseased tree' class.
Row highlighted in grey shows the most accurate classification.

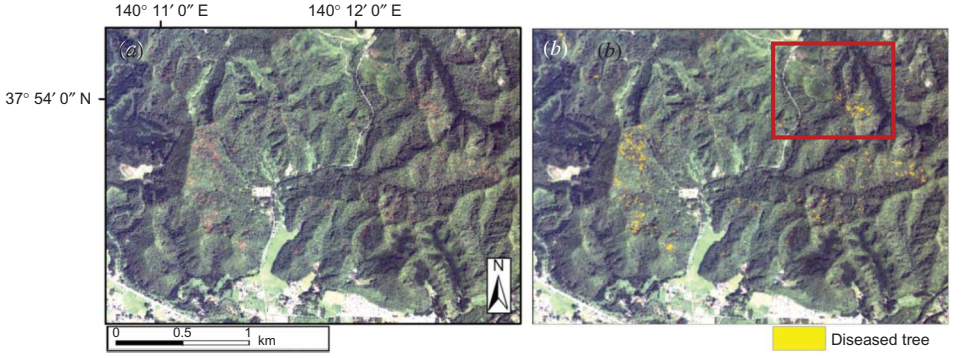

Figure 2. True colour QuickBird image of the entire study area (*a*) and the classified diseased trees overlaid on the image (*b*). The red rectangle shows the location of the inset map in Figure 3.

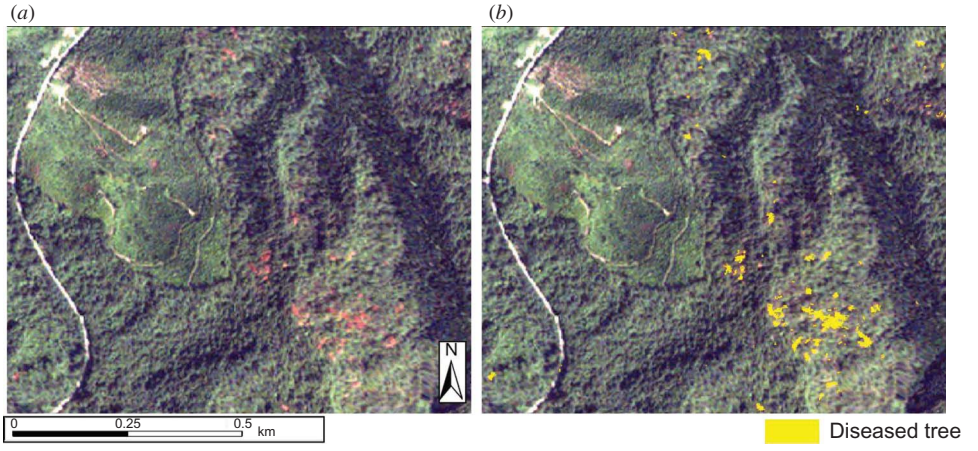

Figure 3. True colour QuickBird image of a part of the study area (*a*) and the classified diseased trees overlaid on the image (*b*). Diseased oak trees are located in the light green areas (broadleaf forest) and diseased pine trees are found in the darker green areas (pine forest).

2012; Johnson 2013). However, our finding that the most accurate classifications were achieved when all segmentation levels were used for multiscale classification contrasted with those of Johnson (2013), who found that including the undersegmented levels in the multiscale classification led to lower classification accuracy. The different findings in this study may be due to our different approach to collecting training data. Johnson (2013) collected training segments from the finest segmentation level and used the segments that contained these training segments as the training data for the coarser segmentation levels (e.g. scale 20 segments were used for training scale 20 classification, etc.). The disadvantage of this approach was that many training segments were undersegmented in the coarsest segmentation levels, so the posterior probability estimates of segments in these levels were not very accurate (since the undersegmented training segments were not truly representative of the objects of interest). We recommend the approach used in this study for training data collection as it should provide better posterior probability estimates (and thus higher classification accuracy for the multiscale data set).

5. Conclusions

In this study, we found that (1) performing SMOTE prior to SVM classification led to fewer omission errors (i.e. a higher producer's accuracy) for the 'Diseased tree' class; (2) a multiscale object-based classification approach outperformed the single-scale approach in all cases; and (3) use of a hybrid IHS-SFIM pansharpening approach led to an increase in overall accuracy of 6% and an increase in producer's accuracy of 18.7% for the 'Diseased tree' class in the final multiscale classification. Based on the high user's accuracy (96.6%) and producer's accuracy (92.5%) for the 'Diseased tree' class that our proposed classification method achieved, it may provide a viable method for detecting JPW and JOW in forested areas of Japan, which is important for preventing further spreading of diseases.

In regard to training data collection, we found that it was time consuming to acquire training samples for the minority class, 'Diseased tree', because the diseased trees were scattered and the training segments needed to accurately match the boundary of a diseased tree (since the training segments should be representative of the land cover of interest). On the other hand, we could acquire training samples for the 'Other' class very quickly by simply identifying a few locations with no diseased trees and take several hundred training samples at each of these locations. Based on our findings, we make some general recommendations for future remote sensing studies. First, we recommend SMOTE (or other minority class oversampling techniques) for binary classification tasks when it is easy to acquire a large number of training samples for the majority class. We also recommend a multiscale object-based classification approach for binary classification of high-resolution imagery rather than a single-scale approach. Finally, a hybrid pansharpening approach is recommended to obtain spatially and spectrally accurate image segments.

For future research, it would be interesting to test our proposed classification approach with other classification algorithms that also provide posterior probability estimates (e.g. relevance vector machines, random forests, neural networks) to allow for a comparison with SVM. It would also be interesting to test other multiscale classification approaches (e.g. Bruzzone and Carlin 2006; Duro, Franklin, and Dubé 2012) for mapping diseased trees. In our study, we assigned all diseased trees to a single class, but since it may also be useful to map each type of diseased tree separately, our methods could also be tested for mapping JPW and JOW as separate classes. In this case, an oversampling technique for multi-class classification rather than binary classification should be used, such as the Diverse Ensemble Creation by Oppositional Relabelling of Artificial Training Examples (DECORATE) technique (Melville and Mooney 2004). Finally, it is necessary to test our

proposed classification method for detecting other types of plant diseases and using other types of imagery to further evaluate its potential applications.

Acknowledgements

We would like to thank the Japan Society for the Promotion of Science (JSPS) for supporting this research under the JSPS Postdoctoral Fellowship for Foreign Researchers.

References

Blaschke, T., C. Burnett, and A. Pekkarinen. 2004. "New Contextual Approaches Using Image Segmentation for Object-based Classification." In *Remote Sensing Image Analysis: Including the Spatial Domain*, edited by F. De Meer and S. de Jong, 211–236. Dordrecht: Kluver Academic Publishers.

Bruzzone, L., and L. Carlin. 2006. "A Multilevel Context-based System for Classification of Very High Spatial Resolution Images." *IEEE Transactions on Geoscience and Remote Sensing* 44: 2587–2600.

Burges, C. 1998. "A Tutorial on Support Vector Machines for Pattern Recognition." *Data Mining and Knowledge Discovery* 2: 121–167.

Chawla, N., K. Bowyer, L. Hall, and W. Kegelmeyer. 2002. "SMOTE: Minority Over-Sampling Technique." *Journal of Artificial Intelligence Research* 16: 341–378.

Dellerba, M. 2010. "Wilt Oak Trees Detection Using Hyperspectral Images with Neural Networks and GTI Method". Master's thesis, Politecnico di Milano, Italy.

Duro, D., S. Franklin, and M. Dubé. 2012. "Multi-scale Object-based Image Analysis and Feature Selection of Multi-sensor Earth Observation Imagery Using Random Forests." *International Journal of Remote Sensing* 33: 4502–4526.

Food and Agriculture Organization of the United Nations Regional Office for Asia and the Pacific. 2010. "Japan Forestry Outlook Study." In *Asia-Pacific Forestry Sector Outlook Study II Working Paper Series*, 9–10. Working Paper No. APFSOS II/WP/2010/30.

Foody, G., and A. Mathur. 2004. "A Relative Evaluation of Multiclass Image Classification by Support Vector Machines." *IEEE Transactions on Geoscience and Remote Sensing* 42: 1335–1343.

Futai, K. 2003. "Role of Asymptomatic Carrier Trees in Epidemic Spread of Pine Wilt Disease." *Journal of Forest Research* 8: 253–260.

Hall, M., E. Frank, G. Holmes, B. Pfahringer, P. Reutmann, and I. Witten. 2009. "The WEKA Data Mining Software: An Update." *SIGKDD Explorations* 11: 1–18.

Haralick, R., K. Shanmugam., and I. Dinstein. 1973. "Textural Features for Image Classification." *IEEE Transactions on Systems, Man, and Cybernetics SMC-3* 6: 610–621.

Hastie, T., and R. Tibshirani. 1998. "Classification by Pairwise Coupling." *The Annals of Statistics* 26: 451–471.

Johnson. B. 2013. "High-resolution Urban Land-cover Classification Using a Competitive Multi-scale Object-based Approach." *Remote Sensing Letters* 4: 131–140.

Johnson, B., R. Tateishi, and N. Hoan. 2012. "Satellite Image Pansharpening Using a Hybrid Approach for Object-based Image Analysis." *ISPRS International Journal of Geo-Information* 1: 228–241.

Kavzoglu, T., and I. Colkensen. 2009. "A Kernel Functions Analysis for Support Vector Machines for Land Cover Classification." *International Journal of Applied Earth Observation and Geoinformation* 11: 352–359.

Kobayashi, F., A. Yamane, and T. Ikeda. 1984. "The Japanese Pine Sawyer Beetle as the Vector of the Pine Wilt Disease." *Annual Review of Entomology* 29: 115–135.

Komura, R., M. Kubo, N. Kamata, and K. Muramoto. 2003. "Analysis of Forest Damage by Harmful Insects on Mt. Kariyasu." SICE Annual Conference 1, 437–440, Fukui, August 4–6.

Kubono, T., and S. Ito. 2002. "Raffaelea Quercivora sp. nov. Associated with Mass Mortality of Japanese Oak, and the Ambrosia Beetle (Platypus Quercivorus)." *Mycoscience* 43: 255–260.

Lee, S., and H. Cho. 2006. "Detection of the Pine Trees Damaged by Pine Wilt Disease Using High Spatial Remote Sensing Data." Proceedings of the ISPRS Commission VII Symposium 'Remote Sensing: From Pixels to Processes', Volume XXXVI, Part 7, edited by N. Kerle and A. Skidmore, Enschede, May 8–11.

Li, W., Q. Guo, and C. Elkan. 2011. "A Positive and Unlabeled Learning Algorithm for One-class Classification of Remote-sensing Data." *IEEE Transactions on Geoscience and Remote Sensing* 49: 717–725.

Liu, J. 2000. "Smoothing Filter-based Intensity Modulation: A Spectral Preserve Image Fusion Technique for Improving Spatial Details." *International Journal of Remote Sensing* 21: 3461–3472.

Manevitz, L., and M. Yousef. 2001. "One-class SVMs for Document Classification." *Journal of Machine Learning Research* 2: 139–154.

Melville, P., and R. Mooney. 2004. "Creating Diversity in Ensembles Using Artificial Data." *Information Fusion* 6: 99–111.

Mountrakis, G., J. Im, and C. Ogole. 2011. "Support Vector Machines in Remote Sensing: A Review." *ISPRS Journal of Photogrammetry and Remote Sensing* 66: 247–259.

Muñoz-Marí, J., F. Bovolo, L. Gómez-Chova, L. Bruzzone, and G. Camps-Valls. 2010. "Semisupervised One-class Support Vector Machines for Classification of Remote Sensing Data." *IEEE Transactions on Geoscience and Remote Sensing* 48: 3188–3197.

Myint, S., P. Gober, A. Brazel, S. Grossman-Clarke, and Q. Weng. 2011. "Per-pixel vs. Object-based Classification of Urban Land Cover Extraction Using High Spatial Resolution Imagery." *Remote Sensing of Environment* 115: 1145–1161.

Ohta, K., K. Hoshizaki, K. Nakamura, A. Nagaki, Y. Ozawa, A. Nikkeshi, A. Makita, K. Kobayashi, and O. Nakakita. 2012. "Seasonal Variations in the Incidence of Pine Wilt and Infestation by Its Vector, Monochamus Alternatus, Near the Northern Limit of the Disease in Japan." *Journal of Forest Research* 17: 360–368.

Padwick, C., M. Deskevich, F. Pacifici, and S. Smallwood. 2010. "Worldview-2 Pansharpening." American Society for Photogrammetry and Remote Sensing Annual Conference 2010: Opportunities for Emerging Geospatial Technologies, San Diego, CA, April 26–30.

Schowengerdt, R. 2006. *Remote Sensing: Models and Methods for Image Processing*, 371–378. Orlando, FL: Academic Press.

Scott, C., and G. Blanchard. 2009. "Novelty Detection: Unlabeled Data Definitely Help." Proceedings of the 12th International Conference on Artificial Intelligence and Statistics (AISTATS), edited by D. Dyk and M. Welling, Clearwater Beach, FL, April 16–18.

Solberg, A., and R. Solberg. 1996. "A Large-Scale Evaluation of Features for Automatic Detection of Oil Spills in ERS SAR Images." International Geoscience and Remote Sensing Symposium, 1484–1486, Lincoln, NE, May 27–31.

Tang, Y., Y. Zhang, N. Chawla, and S. Krasser. 2009. "SVMs Modeling for Highly Imbalanced Classification." *IEEE Transactions on Systems, Man, and Cybernetics-Part B: Cybernetics* 39: 281–288.

Trimble. 2012. *eCognition Developer 8.7.1 Reference Book*, 34–38. München: Trimble Germany GmbH.

Tu, T., C. Hsu, P. Tu, and C. Lee. 2012. "An Adjustable Pan-Sharpening Approach for IKONOS/QuickBird/GeoEye-1/WorldView-2 Imagery." *IEEE Journal of Selected Topics in Applied Earth Observations and Remote Sensing* 5: 125–134.

Tu, T., P. Huang, C. Hung, and C. Chang. 2004. "A Fast Intensity-Hue-Saturation Fusion Technique with Spectral Adjustment for IKONOS Imagery." *IEEE Geoscience and Remote Sensing Letters* 1: 309–312.

Tu, T., Y. Lee, C. Chang, and P. Huang. 2005. "Adjustable Intensity-Hue-Saturation and Brovey Transform Fusion Technique for IKONOS/QuickBird Imagery." *Optical Engineering* 44: 1–10.

Tu, T., S. Su, H. Shyu, and P. Huang. 2001. "A New Look at IHS-Like Image Fusion Methods." *Information Fusion* 2: 177–186.

Uto, K., T. Massaki, Y. Kosugi, G. Saito, and T. Ogata. 2011. "Band Selection for Japanese Oak Wilt Extraction in Autumnal Tints of Forest Based on NWI." 3rd Workshop on Hyperspectral Image and Signal Processing: Evoloution in Remote Sensing (WHISPERS), 1–4, Lisbon, June 6–9.

Yu, Q., P. Gong, N. Clinton, G. Biging, M. Kelly, and D. Schirokauer. 2006. "Object-based Detailed Vegetation Classification with Airborne High Spatial Resolution Remote Sensing Imagery." *Photogrammetric Engineering and Remote Sensing* 72: 799–811.

Zhou, W., and A. Troy. 2009. "Development of an Object-Based Framework for Classifying and Inventorying Human-Dominated Forest Ecosystems." *International Journal of Remote Sensing* 30: 6343–6360.